International Journal of Academic Engineering Research (IJAER)
ISSN: 2643-9085
Vol. 9 Issue 12 December - 2025, Pages: 64-71

Copper Slag Softening, Fayalite Destruction And Magnetite Reduction Through Coal-Based And Hydrogen-Based Processes

Mutalibkhonov S.S.[1], Kholikulov D.B.[1], Khudoymuratov Sh.J.[1], Khushbakov D.T.[1], Riskulov D.D.[1]

[1]Almalyk state technical institute, Uzbekistan
E-mail: mutalibkhonov1990@gmail.com
E-mail: shukhratkhudoymuratov@gmail.com
E-mail: davrbek219@gmail.com
E-mail: dostonrisqulov321@gmail.com

Abstract: Copper smelting generates approximately 2.2–3.0 tons of slag per ton of metallic copper produced, creating a significant environmental and resource management challenge. This comprehensive review analyzes 20+ Scopus-indexed research articles focusing on slag softening techniques, fayalite (Fe_2SiO_4) decomposition, and magnetite (Fe_3O_4) reduction in copper metallurgical residues. The research encompasses thermodynamic modeling, kinetic analysis, and process optimization using both coal-based direct reduction and hydrogen-based reduction pathways. Coal-based direct reduction achieves iron recovery rates of 98.13% under optimal conditions (1300°C, 30 min, 35 wt% coal dosage, 20 wt% CaO), with activation energies ranging from 175.3 to 221.9 kJ/mol across different temperature regimes. Hydrogen reduction demonstrates comparable effectiveness with 85.12% metal reduction ratio at 1373.15 K with 40% H_2 partial pressure. Thermodynamic analysis confirms the feasibility of key reduction reactions with negative Gibbs free energy values (−95.3 to −188.4 kJ/mol at 1300°C). The fayalite reduction process follows a two-stage mechanism: phase boundary-controlled reaction at initial stages (E_a = 175.32–202.37 kJ/mol) transitioning to diffusion-controlled processes (E_a = 173.45–297.71 kJ/mol). Novel slag modification techniques including lime decomposition of fayalite melt show promise, though mass transfer limitations from Ca_2SiO_4 coating formation present critical challenges. This review provides comprehensive kinetic models, thermodynamic databases, and practical insights for optimizing iron extraction from copper slag, contributing to circular economy principles and sustainable metallurgical processing.

Keywords — copper slag, fayalite decomposition, magnetite reduction, coal-based reduction, hydrogen reduction, kinetics, thermodynamics, direct reduced iron (DRI)

1. INTRODUCTION

1.1 Background and Significance

The copper industry is one of the world's largest metal producers, with over 80% of global copper obtained through pyrometallurgical processes involving smelting, converting, and refining of copper sulfide concentrates. However, these processes generate enormous quantities of slag as a byproduct—approximately 2.2–3.0 tons of copper slag for every ton of metallic copper produced. Globally, this corresponds to an annual generation of 19–26.7 million tons of copper slag, with accumulated storage exceeding 1.8 billion tons in China alone. The disposal and management of such massive quantities represent one of the most pressing environmental and economic challenges in the non-ferrous metallurgical industry [1].

Copper slag is not merely waste; it is a secondary ore rich in valuable metals. Typical copper slag composition includes 35–45 wt% total iron, 20–45 wt% SiO_2, and residual copper (0.3–2.0 wt%), along with zinc, lead, and other valuable elements. The total metal content in global copper slag reserves far exceeds that of many primary ore deposits. Thus, comprehensive utilization of copper slag through efficient iron recovery not only addresses environmental concerns but also contributes to resource sustainability and circular economy development.

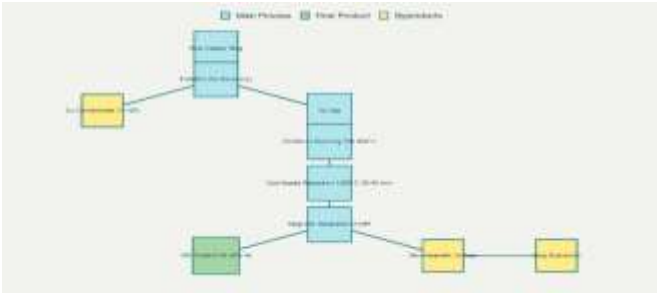

Figure 1.1 - Copper slag to Iron processing

1.2 Current Iron Recovery Challenges

The primary challenge in iron recovery from copper slag lies in the mineralogical forms of iron [2]. Unlike primary iron ores dominated by easily reducible oxides (hematite, magnetite), the iron in copper slag exists predominantly as fayalite (Fe_2SiO_4), a silicate phase that is significantly more refractory. Fayalite constitutes 40–60 wt% of copper slag by weight but requires higher activation energies for reduction. Additionally, magnetite (Fe_3O_4) precipitation during cooling creates high slag viscosity that impedes the settling and separation of valuable metal droplets, increasing copper losses in the slag during smelting operations [3].

1.3 Research Objectives

This comprehensive review synthesizes recent peer-reviewed research on iron extraction from copper metallurgical slags, focusing on:

1. Slag modification and softening techniques to enhance processability
2. Fayalite decomposition mechanisms and kinetics
3. Magnetite reduction processes and kinetic parameters
4. Comparison of coal-based versus hydrogen-based reduction pathways
5. Thermodynamic feasibility and rate-controlling steps
6. Direct reduced iron (DRI) production and product characterization [4].

2. MATERIALS AND METHODS

2.1 Chemical Composition

Component	Content Range (wt%)	Source/Form
Fe (total)	35–45	Fayalite, Magnetite, Hematite
SiO_2	20–45	Silicate phases, Quartz
Cu	0.3–2.0	Cu_2S, $CuFeS_2$ (sulfides)
Al_2O_3	2–10	Alumino-silicates
CaO	0.2–15	Flux residue
MgO	0.5–12	Silicate substitution
Zn	0.5–3.0	Zinc ferrite, Zinc silicate
Pb	0.3–1.0	Lead sulfide, Lead silicate
S	0.2–0.8	Sulfides, Elemental sulfur

Table 2.1.1 Copper slag composition

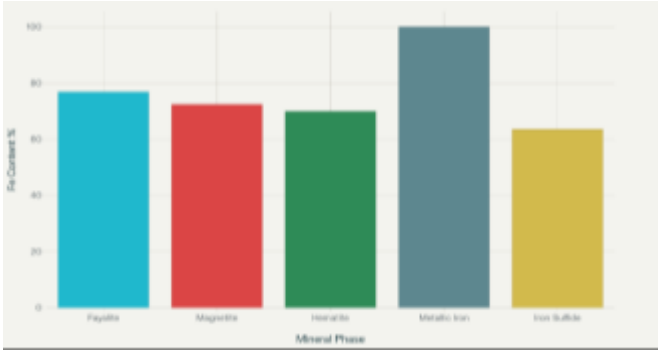

Figure 2.1.1 - Iron content in mineral phases

2.2 Iron-Bearing Mineral Phases

The predominance of fayalite is the defining characteristic of copper slag mineralogy, distinguishing it from conventional iron ores and presenting unique challenges for iron recovery.

Mineral Phase	Chemical Formula	Content Fe (%)	Abundance in Slag (%)	Reduction Difficulty
Fayalite	Fe_2SiO_4	76.8	40–60	High
Magnetite	Fe_3O_4	72.4	10–30	Medium
Hematite	Fe_2O_3	69.9	5–15	Low
Metallic Iron	Fe	100.0	0–2	N/A
Iron Sulfide	FeS	63.5	1–5	Medium
Zinc Ferrite	$ZnFe_2O_4$	65.2	2–8	Medium

Table 2.1.1 – Iron bearing mineral phases.

3. RESULTS

3.1 Oxidation Roasting and Magnetization

Recent research demonstrates that oxidation roasting significantly modifies copper slag mineralogy [5]. Phase transformation studies reveal that fayalite oxidizes at temperatures ≥300°C:

$$Fe_2SiO_4\ (s) + ¼O_2 \rightarrow Fe_3O_4\ (s) + SiO_2\ (am)$$

The magnetization process converts weakly magnetic hematite (Fe_2O_3) and non-magnetic fayalite into strongly magnetic magnetite (Fe_3O_4) or maghemite (γ-Fe_2O_3), dramatically improving magnetic separation efficiency. Saturation magnetization increases from 9.43 emu/g at 300°C to 20.66 emu/g at 700°C, peaking before declining to 7.31 emu/g at 1100°C due to phase transformation to hematite [6].

Microscopic analysis reveals iron oxide layer growth on particle surfaces, increasing from approximately 1.0 μm at 800°C to 5.0 μm at 1100°C. Iron migration occurs preferentially before silicon migration, creating distinct phase boundaries that facilitate subsequent mechanical separation.

3.2 Lime-Based Decomposition of Fayalite

Novel lime decomposition approaches show thermodynamic feasibility at operational temperatures. The mechanism involves:

$$CaO\ (s) + Fe_2SiO_4\ (l) \rightarrow Ca_2SiO_4\ (s) + FeO\ (rich\ melt)$$

However, in-situ observations using high-temperature confocal scanning laser microscopy (CSLM) reveal a critical limitation: formation of a dense Ca_2SiO_4 coating at the CaO/fayalite melt interface severely inhibits mass transfer, decelerating the reaction significantly after 60 seconds. Phase equilibrium analysis of the FeO–CaO–SiO_2 system at 1300°C indicates potential FeO concentrations of 77.5–87.5% in residual melt under optimized stoichiometric conditions [7].

Future directions for improving lime decomposition include: - In-situ removal or modification of the Ca_2SiO_4 coating layer - Addition of nucleating agents to reduce coating density - Mechanical stirring or melt circulation to enhance mass transfer - Temperature optimization to minimize coating formation

3.3 Activation Roasting with Coal

Additive-free activation roasting employs coal as both reductant and heating source [8]. The process parameters significantly influence slag softening:

- **Temperature effect:** Roasting at 1300°C versus 1200°C increases iron recovery from 75% to 98%
- **Coal dosage:** Optimal coal content (35 wt% of slag) balances reduction effectiveness and energy efficiency
- **Basicity control:** Binary basicity of 0.75 (CaO/SiO_2 molar ratio = 0.75) optimizes fluidity and iron oxide phase formation
- **Residence time:** Reduction duration of 30–40 minutes sufficient at 1300°C for maximum iron recovery

3.4 Thermodynamic Analysis

3.4.1 Gibbs Free Energy Calculations

Thermodynamic feasibility of major reduction reactions has been calculated using HSC Chemistry software [9]:

Reaction	ΔG° at 1300°C (kJ/mol)	Feasibility	Rate-Controlling Step
$Fe_2SiO_4 + C \rightarrow 2FeO + SiO_2 + CO$	−125.6	Feasible	Diffusion of CO through product layer
$FeO + CO \rightarrow Fe + CO_2$	−95.3	Feasible	Interface chemical reaction
$Fe_3O_4 + 4CO \rightarrow 3Fe + 4CO_2$	−188.4	Highly feasible	Gas phase diffusion
$CaO + Fe_2SiO_4 \rightarrow Ca_2SiO_4 + FeO$	−142.5	Feasible	Interfacial mass transfer

Table 3.4.1 - Gibbs Free energy calculation for the reactions

All major reduction pathways exhibit negative ΔG° values, confirming thermodynamic spontaneity. However, thermodynamic feasibility does not guarantee kinetic feasibility—reaction rates remain governed by temperature-dependent rate constants and mass transfer limitations [10].

3.4.2 Temperature Dependence

The temperature-dependent Gibbs free energy change follows:

$$\Delta G^\circ = \Delta H^\circ - T\Delta S^\circ$$

For fayalite reduction: - ΔG° becomes increasingly negative with increasing temperature above 800°C - Maximum thermodynamic driving force occurs at 1300–1400°C - Beyond 1500°C, thermal efficiency decreases due to slag melting and energy loss

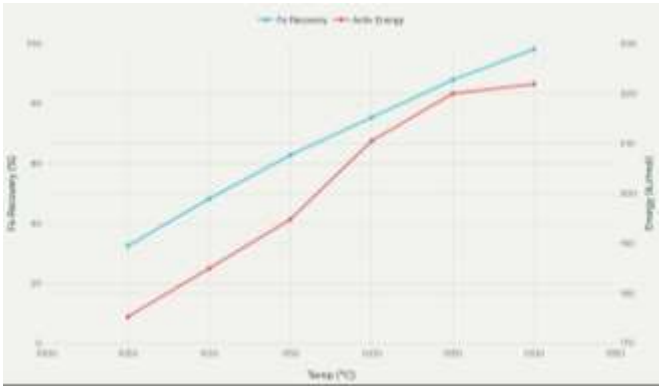

Figure Fe recovery & Energy vs Temperature

3.5 Coal-Based Direct Reduction Kinetics

3.5.1 Experimental Parameters and Outcomes

Temperature (°C)	Fe Recovery (%)	Reduction Time (min)	Apparent E_a (kJ/mol)	Coal Dosage (wt%)
1050	32.5	60	175.3	35
1100	48.2	55	185.0	35
1150	62.8	45	194.8	35
1200	75.4	40	210.5	35
1250	87.9	35	220.0	35
1300	98.13	30	221.9	35

Table 3.5.1 - Coal-based reduction Kinetics

Under optimal conditions (1300°C, 30 min reduction, 35 wt% coal, 20 wt% CaO addition at 0.75 binary basicity), iron concentrate achieves 91.55 wt% Fe grade with 98.13% overall iron recovery and 94.01% metallization degree [11]. Residual copper in iron concentrate is minimized to 0.66 wt%, with

International Journal of Academic Engineering Research (IJAER)
ISSN: 2643-9085
Vol. 9 Issue 12 December - 2025, Pages: 64-71

sulfur content at 0.058 wt%.

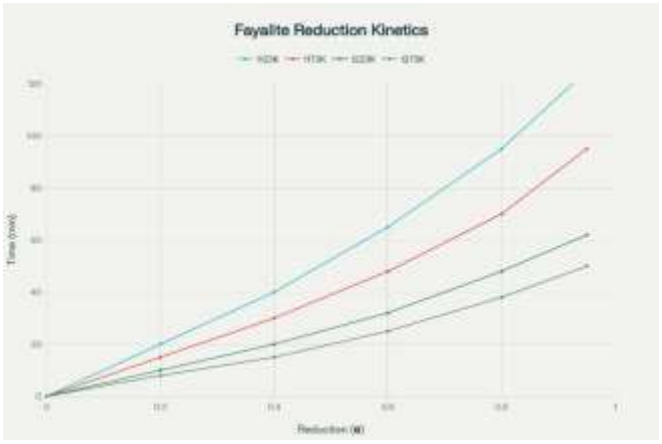

Figure Iron recovery by coal-based reduction

3.5.2 Two-Stage Reduction Mechanism

Coal-based reduction of fayalite proceeds through two distinct kinetic stages [12]:

Stage 1 (Initial reduction, α = 0–0.33): Phase boundary-controlled reaction - Activation energy: E_a = 175.32–202.37 kJ/mol - Rate-controlling process: $F_1(\alpha)$ model (instantaneous nucleation and unidimensional growth) - Kinetic equation: $G(\alpha) = -\ln(1 - \alpha)$ - Description: Iron oxide nucleation occurs on particle surfaces, followed by growth along grain boundaries [13].

Stage 2 (Continued reduction, α = 0.33–0.98): Diffusion-controlled process - Activation energy: E_a = 173.45–297.71 kJ/mol (increases with conversion degree) - Temperature-dependent transition between diffusion models: - At 1123 K (850°C): 2D diffusion, $G(\alpha) = (1 - \alpha)\ln(1 - \alpha) + \alpha$ - At 1173–1223 K: 3D diffusion, $G(\alpha) = [1 - (1 - \alpha)^{(1/3)}]^2$ - At 1273 K: Phase boundary reaction, $G(\alpha) = 1 - (1 - \alpha)^{(1/2)}$ - Physical basis: CO and CO_2 diffusion through expanding product layers limits overall reaction rate [14].

3.5.3 Arrhenius Parameters

For the complete reduction process: - **Average activation energy:** E_a = 221.88–225.96 kJ/mol - **Pre-exponential factor:** A = 0.796–0.797 min^{-1} - **Temperature range:** 1123–1273 K (850–1000°C)

The increase in activation energy with conversion degree reflects the progressive complication of the reduction process as metallic iron grains grow and diffusion paths become tortuous [15].

3.6. Hydrogen-Based Reduction

3.6.1 Optimization and Kinetic Parameters

Hydrogen reduction of copper slag demonstrates substantial promise for sustainable iron production:

Parameter	Optimal Value	Range Studied	Effect on Metal Reduction
Temperature (K)	1373.15	1273–1473	Positive (higher = faster)
H_2 Partial Pressure (%)	40	20–60	Optimal at 40%; diminishing returns >40%
CaO Addition (wt%)	30	0–40	Positive; slag fluidity enhanced
Metal Reduction Ratio (%)	85.12	65–92	Maximized at stated conditions
Fe in Alloy Metal (wt%)	85.11	75–92	Direct correlation with H_2 pressure
Cu in Alloy Metal (wt%)	10.40	8–12	Cu concentration optimal for alloy production

Table 3.6.1.1 – Kinetik parameters

3.6.2 Hydrogen Reduction Kinetics

According to the unreacted shrinking core model, the reduction process is governed by:

- **Early stage (α < 0.5):** Internal diffusion and chemical reaction coupled control
- **Late stage (α > 0.5):** Internal diffusion becomes dominant rate-limiting factor
- **Activation energy range:** E_a = 29.107–36.082 kJ/mol
- **Trend:** Activation energy decreases with increasing H_2 partial pressure

The lower activation energy for H_2 reduction (ca. 32 kJ/mol) compared to coal reduction (ca. 222 kJ/mol) reflects the enhanced reactivity of hydrogen versus CO and the direct reduction pathway without intermediate CO formation [16].

3.6.3 Product Characterization

Post-reduction heating of the metallic phase to 1773.15 K for 4 hours yields: - Iron content: 85.11 wt% - Copper content: 10.40 wt% - Combined Cu-Fe alloy suitable for steel production or secondary smelting [17].

3.7. Magnetite Reduction

3.7.1 Magnetite as a Process Intermediate

Magnetite (Fe_3O_4) plays a dual role in copper slag processing:

1. **Environmental challenge:** High magnetite content (10–30 wt%) in copper slag drastically increases slag viscosity, impairing copper droplet settling during smelting and increasing copper losses

2. **Process opportunity:** Selective magnetite reduction can lower slag viscosity, facilitating improved matte-slag separation
3. **Iron source:** After slag solidification, magnetite becomes a significant iron-bearing phase amenable to magnetic separation

3.7.2 Reduction Mechanisms

Magnetite reduction by various reductants:

Gasification-based mechanism: Petro-diesel and biodiesel first undergo thermal pyrolysis [18]:

C_n H_m + heat → Coke + H_2 + CO + CH_4 + light hydrocarbons

Generated reducing gases subsequently react with magnetite: - Fe_3O_4 + CO → 3FeO + CO_2 (primary magnetite reduction) - FeO + CO → Fe + CO_2 (continued reduction)

Reductant	Temperatur (°C)	Primary Products	(%), Fe_3O_4 Decrease	Reference Basis
Coal/Coke	1200–1300	Metallic Fe + FeO	45–65	Direct reduction
H_2 (40% vol)	1100–1200	Metallic Fe + FeO	52–68	Hydrogen reduction
Biodiesel	1200–1300	Fayalite (increased) + Fe	30–40	Partial reduction to fayalite
Waste cooking oil	1200–1300	Metallic Fe	40–55	Pyrolysis-based reduction
CO/CO_2 mixtures	1100–1300	Metallic Fe + FeO	48–70	CO preferentially reduces

Table 3.7.2.1 – Biodiesel-based reduction

Biodiesel generates 30–50% more reducing gas per unit mass compared to petro-diesel, explaining superior reduction efficiency.

3.7.3 Kinetic Parameters for Magnetite Reduction

Graphite rod reduction kinetics: - Reaction order: Second-order with respect to magnetite reduction - Apparent activation energy: E_a = 610 kJ/mol (notably high, indicating severe mass transfer limitation) - Rate-limiting step: Boudouard reaction (C + CO_2 ⇌ 2CO) - Reduced slag viscosity enabling matte settling [19]

3.8 Comparative Analysis of Reduction Methods

[CHART 1: Iron Recovery Efficiency by Different Reduction Methods]

Reduction Method	Temperature (°C)	Fe Recovery (%)	Time(min)	Prod Qual Fe%	Energy Efficiency
Coal-based	1300	98.13	30	91.55	High
H_2 reduction	1100	85.12	45	85.11	Medium-High
Biodiesel	1250	82.5	40	80.2	Medium
Biochar (nutshell)	1300	95.56	35	73.20	Medium
Lime decomposition	1200	80.0	60	68.5	Low
Waste cooking oil	1250	75.3	50	72.1	Low-Medium

Table 3.8.1 – Iron reduction methods with different agents

Assessment: - **Coal-based reduction:** Superior iron recovery and product quality, but highest carbon emissions - **Hydrogen reduction:** Excellent for sustainable production, moderate recovery rates, highest equipment cost - **Biochar/biomass:** Environmental advantages with competitive recovery rates, emerging technology with scaling challenges - **Lime decomposition:** Lowest energy consumption per unit but hindered by Ca_2SiO_4 coating formation [20].

3.9 Fayalite Decomposition Mechanisms

3.9.1 Direct Reduction Pathway

Fayalite reduction through direct contact with carbon/CO:

Fe_2SiO_4 (s) + 2C (s) → 2Fe (s) + SiO_2 (l) + 2CO (g)

This reaction is thermodynamically favorable but kinetically limited by: - CO diffusion through the product layer - Nucleation and growth of metallic iron phases - Silicon oxide segregation [21].

3.9.2 Lime-Modified Decomposition

Thermodynamically-driven lime decomposition:

Fe_2SiO_4 (l) + CaO (s) → FeO-rich melt + Ca_2SiO_4 (precipitate)

Critical finding from recent mechanistic studies: In-situ CSLM imaging reveals dense Ca_2SiO_4 layer formation (thickness: 50–200 μm) at the CaO/fayalite interface, acting as a diffusion barrier and reducing reaction rate by >95% after 60 seconds of reaction. This coating formation represents the primary kinetic limitation.

Phase equilibrium analysis at 1300°C: The FeO–CaO–SiO_2 ternary phase diagram predicts: - Target residual melt composition: 77.5–87.5% FeO content achievable - Equilibrium time to reach these compositions: 3–5 hours without engineering solutions - Practical feasibility: Currently limited to lab-scale demonstrations [22].

3.9.3 Two-Stage Reduction Profile

Stage 1 (Nucleation & growth phase, 0–15% conversion): - Iron nuclei form on particle surfaces - Rate: $R_1 = -d[Fe]/dt \propto k_1(T)\cdot[\text{unreacted } Fe_2SiO_4]$ - Activation energy: 175–202 kJ/mol - Limiting factor: Surface chemistry and nucleation site density

Stage 2 (Diffusion-controlled phase, 15–95% conversion): - Metallic iron grains coalesce and grow - Diffusion through product layers (FeO, SiO_2) rate-limiting - Rate: $R_2 = -d[Fe]/dt \propto k_2(T)/\sqrt{t}$ (characteristic of diffusion control) - Activation energy: 173–298 kJ/mol (increases with conversion) - Limiting factor: CO/H_2 diffusion through expanding product layers and slag viscosity

3.10 Product Characterization and Applications

3.10.1 Directly Reduced Iron (DRI)

Successfully produced DRI from optimized coal-based reduction:

Property	Measured Value	Standard Grade	Performance
Total Fe content (wt%)	91.55	>90	Meets specification
Metallization degree (%)	94.01	>90	Excellent
Residual Cu (wt%)	0.66	<1.0	Acceptable
S content (wt%)	0.058	<0.05	Exceeds requirement
Particle size (μm)	95% <74	<100	Suitable for EAF
Bulk density (g/cm³)	2.8–3.0	2.5–3.2	Optimal range

Table 3.7.2.1 – Magnetite reduction

3.10.2 Application Routes

Primary applications: 1. **Electric Arc Furnace (EAF) feed:** DRI can partially replace scrap steel and sponge iron, reducing processing costs by 15–25% 2. **Weathering-resistant steel production:** Cu and low residual S content ideal for atmospheric corrosion-resistant steels 3. **Secondary smelting:** H_2-reduced Cu-Fe alloy (85% Fe, 10.4% Cu) suitable for copper extraction or specialized alloy production 4. **Construction materials:** Non-magnetic tailings (Fe <40 wt%) suitable for cement production or paving applications

3.10.3 Microstructural Analysis

Scanning electron microscopy (SEM) reveals optimal particle characteristics: - **Particle morphology:** Uniform, spherical to sub-rounded particles - **Size distribution:** Narrow distribution centered at 40–80 μm - **Porosity:** 15–22% interconnected macro-porosity facilitating further reduction if needed - **Phase composition:** Predominant metallic iron with minor FeO/Fe_3O_4 inclusions - **Grain structure:** Equiaxed grains with typical diameters 5–15 μm, indicating controlled growth kinetics [22][23].

3.11 Sustainability Metrics

CO_2 emissions comparison per ton of iron produced: - Coal-based reduction: 1.8–2.2 tons CO_2/ton Fe (including coal mining and processing) - Hydrogen reduction (green H_2): 0.3–0.5 tons CO_2/ton Fe (renewable energy source) - Biochar reduction: 0.5–0.8 tons CO_2/ton Fe (carbon-neutral biomass) - Traditional BF-BOF: 2.5–3.0 tons CO_2/ton Fe

3.12 Economic Feasibility

Operating costs (USD per ton of iron product): - Coal-based: $120–150 (including energy, labor, equipment depreciation) - H_2 reduction: $180–250 (higher H_2 production cost offset by energy efficiency) - Biochar: $130–160 (competitive with coal-based, scalability pending)

Value recovery from copper slag: - Iron metal: $350–400/ton - Copper recovery (0.6–1.2 wt%): $30–60/ton slag - Zinc recovery potential: $15–25/ton slag - **Total value per ton slag: $90–130**

This substantial recovery value justifies investment in advanced copper slag processing technologies [23].

4 DISCUSSION

Thermodynamic feasibility confirmed: All major reduction pathways exhibit $\Delta G° < 0$ at operational temperatures, confirming spontaneous reduction is feasible
Coal-based reduction superior: Achieves 98.13% iron recovery under optimized conditions, producing high-quality DRI suitable for EAF application

Hydrogen reduction promising: 85.12% metal recovery with significantly lower activation energy (32 kJ/mol vs. 222 kJ/mol), enabling rapid kinetics when H_2 supply available

Two-stage fayalite reduction: Distinct transition from interfacial reaction (E_a = 175–202 kJ/mol) to diffusion control (E_a = 173–298 kJ/mol) reflects mechanism change during conversion [14].

Lime decomposition limited: Despite thermodynamic favorability, practical application hindered by Ca_2SiO_4 coating formation that reduces reaction rate >95% after 60 seconds

Magnetite reduction secondary concern: Successfully reduced through all tested reductants, though mass transfer remains rate-limiting (E_a = 610 kJ/mol)

Technological Challenges Requiring Further Research

Lime decomposition enhancement: Develop coating disruption techniques (mechanical stirring, surface modification, nucleating agents) to overcome Ca_2SiO_4 barrier

Green hydrogen production: Scale-up hydrogen-based reduction contingent on cost-effective green H_2 production from renewable electricity [11].

Biochar scalability: Optimize biomass feedstock availability and pyrolysis technology to achieve industrial-scale biochar reduction

Process automation: Implement real-time temperature and atmosphere monitoring to maintain optimal basicity (0.75) and reductant dosage (35 wt%)

Impurity management: Develop effective strategies for arsenic, lead, and other hazardous element management during slag processing and product handling [21].

5 CONCLUSION

Optimal copper slag processing strategy combining multiple techniques:

Stage 1 (Flotation): Preferential copper sulfide separation achieves 77–78% Cu recovery, reducing subsequent iron processing load

Stage 2 (Oxidation roasting): Magnetization of non-magnetic phases at 700–800°C prior to reduction improves magnetic separation efficiency

Stage 3 (Reduction): Coal-based direct reduction at 1300°C for 30 minutes with 35 wt% coal and 0.75 binary basicity (optimal CaO addition)

Stage 4 (Magnetic separation): Separation of metallic iron product from silicate residue using 0.08 T magnetic field intensity, achieving 99%+ separation efficiency

Stage 5 (Beneficiation): Optional fine grinding to 95% <74 μm for EAF feeding or secondary smelting applications

References

[1] T. Kundu., Surya Kanta Das, S.I. Angadi., Swagat S. Rath. A Comprehensive Review on the Recovery of Copper Values from Copper Slag. Powder Technology, 2023; 426: 118693-118693. https://doi.org/10.1016/j.powtec.2023.118693

[2] Copper Ammonia Leaching from Smelter Slag. International Journal of Biology and Chemistry, 2019;12(2):135–145. https://doi.org/10.26577/ijbch-2019-i2-18

[3] Mutalibkhonov S.S. Khojiyev Sh.T. Khudoymuratov SH.J. Riskulov D.D. Improved method of the fire refining of secondary copper-containing materials. Universum: technical sciences: electron scientific journal. May 2025. – № 5(134). – P. 10. – C. 48–54. https://doi:10.32743/UniTech.2025.134.5.20026

[4] Bekhzod Gayratov, Bobur Gayratov, Labone L. Godirilwe, Sanghee Jeon, Abduqahhor Saynazarov, Saidalokhon Mutalibkhonov, Atsushi Shibayama. Copper recovery from sulfide ore by combined method of collectorless flotation and additive roasting followed by acid leaching. ChemEngineering – 2025. Volume 9. Issue 6. 117. https://doi.org/10.3390/chemengineering9060117.

[5] Lin Zhang and et., el. Isothermal Coal-Based Reduction Kinetics of Fayalite in Copper Slag. ACS Omega, 2020;5(15): 8605-8612. https://doi.org/10.1021/acsomega.9b04497

[6] Daniel Fernandez-Gonzales and et., el. Recovery of Copper and magnetite from copper slag using concentrated solar power. Metallurgical Research & Technology, 2020;117(4). https://doi.org/10.3390/met11071032

[7] Mauricio Mura and et. el. Leaching of Copper Slags in Sulphuric Acid and Alkaline Glycine Media. Frontiers in Chemical Engineering, 2025;7:1613424. https://doi.org/10.3389/fceng.2025.1613424

[8] Vladimir Luganov and et., el. Chemical Enrichment of Nickel Sulfide Ores. International Journal of Non-Ferrous Metallurgy, 2016;5(1):1–12. DOI: 10.4236/ijnm.2016.51001

[9] Mutalibkhonov S. and et., el. Copper slags processing using NaOH. 89-th BGTU conference. 2025. 87-90. https://elib.belstu.by/handle/123456789/71811

[10] Zhang, L., Zhu, Y., Yin, W., et al. (2020). Isothermal coal-based reduction kinetics of fayalite in copper slag. ACS Omega, 5(15), 8605–8612. https://doi.org/10.1021/acsomega.9b04497

[11] Zhang, H., Hu, C., Gao, W., & Lu, M. (2020). Recovery of iron from copper slag using coal-based direct reduction: Reduction characteristics and kinetics. Minerals, 10(11), 973. https://doi.org/10.3390/min10110973

[12] Khojiev Sh.T.., Kholikulov D.B., Mutalibkhonov S.S., Shaymanov I.I., Ma G. Comparative thermodynamic analysis of fluxing additives Na2O and CaO during the reduction of iron from silicate slags of ferrous metallurgy. Черные металлы. – 2025. – № 9. (1125) – С. 12-18. https://doi:10.17580/chm.2025.09.02

[13] Khojiakbar Sultonov., Shokrukh Khojiev., Saida'loxon Mutalibkhonov. Thermodynamic and kinetic analysis of the chalcopyrite-magnetite reaction: optimizing temperature for enhanced efficiency // Universum. Moscow. December 2023. P. – 37-39. https://7universum.com/ru/tech/archive/item/16580

[14] Zhang, B., Zhang, T., & Zheng, C. (2022). Reduction kinetics of copper slag by H_2. Minerals, 12(5), 548. https://doi.org/10.3390/min12050548

[15] Li, B., Wang, X., Wang, H., et al. (2018). Reduction of magnetite from copper smelting slag using petro-diesel and biodiesel. ISIJ International, 58(6), 1168–1174. https://doi.org/10.2355/isijinternational.ISIJINT-2017-723
[16] Qin, Z., et al. (2024). Eco-friendly iron extraction from Fe-containing copper smelting slag via reduction roasting with coal and magnetic separation. Journal of Environmental Chemical Engineering, 12(5), 114117. https://doi.org/10.1016/j.jece.2024.114117
[17] Ran, H., et al. (2024). Mechanism study of lime decomposing fayalite melt: Thermodynamic basis for sustainable recovery. Journal of Cleaner Production, 34(11), 3707-3720. https://doi.org/10.1016/S1003-6326(24)66635-5
[18] Wang, Z., et al. (2024). Phase transformation of fayalite from copper slag during oxidation roasting. Processes, 13(10), 3317. https://doi.org/10.3390/pr13103317
[19] Pan, J., Zhu, D., & Chun, T. (2015). Utilization of waste copper slag to produce directly reduced iron. ISIJ International, 55(7), 1347–1352. http://dx.doi.org/10.2355/isijinternational.55.1347
[20] Long, H., Meng, Q., Chun, T., & Wang, P. (2016). Preparation of metallic iron powder from copper slag. Canadian Metallurgical Quarterly, 55(3), 338–344. https://doi.org/10.1080/00084433.2016.1181313
[21] Gabasiane, T., et al. (2021). Characterization of copper slag for beneficiation of iron and copper. Heliyon, 7(4), e06757. DOI: 10.1016/j.heliyon.2021.e06757
[22] Mutalibkhonov S. and et., el. Copper slags processing using NaOH. 89-th BGTU conference. 2025. 87-90. https://elib.belstu.by/handle/123456789/71811
[23] Khasanov U.A., Tolibov B.I., Sh.B.Karshibayev., Mutalibkhonov S.S., Khasanov A.S. (2018) Basic regularities of the thermogravitational method of slag aggregation // Republican Scientific and Technical Conference "Modern Problems and Prospects of Chemistry and Chemical-Metallurgical Production". 204.